

Single-molecule imaging reveals the mechanism of Exo1 regulation by single-stranded DNA binding proteins

Logan R. Myler^{a,b,c,1}, Ignacio F. Gallardo^{a,c,1}, Yi Zhou^{a,b}, Fade Gong^a, Soo-Hyun Yang^{a,b}, Marc S. Wold^d, Kyle M. Miller^a, Tanya T. Paull^{a,b,2}, and Ilya J. Finkelstein^{a,c,2}

^aDepartment of Molecular Biosciences, The University of Texas at Austin, Austin, TX 78712; ^bHoward Hughes Medical Institute, The University of Texas at Austin, Austin, TX 78712; ^cCenter for Systems and Synthetic Biology, The University of Texas at Austin, Austin, TX 78712; and ^dDepartment of Biochemistry, Carver College of Medicine, University of Iowa, Iowa City, IA 52242

Edited by Richard D. Kolodner, Ludwig Institute for Cancer Research, La Jolla, CA, and approved January 14, 2016 (received for review August 20, 2015)

Exonuclease 1 (Exo1) is a 5'→3' exonuclease and 5'-flap endonuclease that plays a critical role in multiple eukaryotic DNA repair pathways. Exo1 processing at DNA nicks and double-strand breaks creates long stretches of single-stranded DNA, which are rapidly bound by replication protein A (RPA) and other single-stranded DNA binding proteins (SSBs). Here, we use single-molecule fluorescence imaging and quantitative cell biology approaches to reveal the interplay between Exo1 and SSBs. Both human and yeast Exo1 are processive nucleases on their own. RPA rapidly strips Exo1 from DNA, and this activity is dependent on at least three RPA-encoded single-stranded DNA binding domains. Furthermore, we show that ablation of RPA in human cells increases Exo1 recruitment to damage sites. In contrast, the sensor of single-stranded DNA complex 1—a recently identified human SSB that promotes DNA resection during homologous recombination—supports processive resection by Exo1. Although RPA rapidly turns over Exo1, multiple cycles of nuclease rebinding at the same DNA site can still support limited DNA processing. These results reveal the role of single-stranded DNA binding proteins in controlling Exo1-catalyzed resection with implications for how Exo1 is regulated during DNA repair in eukaryotic cells.

resection | single-molecule | nuclease | DNA curtains | DNA repair

All DNA maintenance processes require nucleases, which enzymatically cleave the phosphodiester bonds in nucleic acids. Exo1, a member of the Rad2 family of nucleases, participates in DNA mismatch repair (MMR), double-strand break (DSB) repair, nucleotide excision repair (NER), and telomere maintenance (1–3). Exo1 is the only nuclease implicated in MMR, where its 5' to 3' exonuclease activity is used to remove long tracts of mismatch-containing single-stranded DNA (ssDNA) (2, 4–7). In addition, functionally deficient Exo1 variants have been identified in familial colorectal cancers, and Exo1-null mice exhibit a significant increase in tumor development, decreased lifespan, and sterility (8, 9). Exo1 also promotes DSB repair via homologous recombination (HR) by processing the free DNA ends to generate kilobase-length ssDNA resection products (1, 10–12). The resulting ssDNA is paired with a homologous DNA sequence located on a sister chromatid, and the missing genetic information is then restored via DNA synthesis. The central role of Exo1 in DNA repair is highlighted by the large set of genetic interactions between Exo1 and nearly all other DNA maintenance and metabolism pathways (13).

Exo1 generates long tracts of ssDNA in both MMR and DSB repair (3). This ssDNA is rapidly bound by replication protein A (RPA), a ubiquitous heterotrimeric protein that participates in all DNA transactions that generate ssDNA intermediates (14). RPA protects the ssDNA from degradation, participates in DNA damage response signaling, and acts as a loading platform for downstream DSB repair proteins (15–17). RPA also coordinates DNA resection by removing secondary ssDNA structures and by

modulating the Bloom syndrome, RecQ helicase-like (BLM)/DNA2- and Exo1-dependent DNA resection pathways (18–21). Reconstitution of both the yeast and human BLM (Sgs1 in yeast)/DNA2-dependent resection reactions established that RPA stimulates DNA unwinding by BLM/Sgs1 and enforces a 5'-endonuclease polarity on DNA2 (20, 22). However, the effect of RPA on Exo1 remains unresolved. Independent studies using reconstituted yeast proteins reported that RPA could both inhibit (23) and stimulate yeast Exo1 (yExo1) (18). Similarly, human RPA has variously been reported to stimulate (19) or inhibit human Exo1 (hExo1) (4, 5, 21).

In addition to RPA, human cells also encode SOSS1, a heterotrimeric ssDNA-binding complex that is essential for HR (24). SOSS1 consists of INTS3 (SOSSA), hSSB1 (SOSSB1), and C9orf80 (SOSSC) (24–26). SOSSB1 encodes a single ssDNA-binding domain that bears structural homology to *Escherichia coli* ssDNA-binding protein (SSB) (24). SOSS1 foci form rapidly after induction of DNA breaks, and ablation of SOSS1 severely reduces DNA resection, γ H2AX foci formation, and HR at both ionizing radiation- and restriction endonuclease-induced DSBs (12, 24, 25, 27). In vitro, SOSS1 stimulates hExo1-mediated DNA resection and may help to load hExo1 at ss/dsDNA junctions (21). However, the

Significance

Exonuclease 1 (Exo1) is a conserved eukaryotic nuclease that participates in DNA repair and telomere maintenance. Here we use high-throughput single-molecule imaging to examine Exo1 activity on DNA and in the presence of single-stranded DNA binding proteins. We report that both human and yeast Exo1 are processive nucleases but are rapidly turned over by replication protein A (RPA). In the presence of RPA, Exo1 retains limited DNA-processing activity, albeit via a distributive binding mechanism. This rapid turnover by RPA can appear stimulatory or inhibitory in gel-based assays, clarifying conflicting results in the existing literature. RPA-depleted human cells show elevated Exo1 loading but reduced overall DNA resection, underscoring the many roles of RPA in regulating DNA resection in vivo.

Author contributions: L.R.M., I.F.G., T.T.P., and I.J.F. designed research; L.R.M., I.F.G., Y.Z., F.G., and S.-H.Y. performed research; L.R.M., I.F.G., M.S.W., and K.M.M. contributed new reagents/analytic tools; L.R.M., I.F.G., Y.Z., F.G., M.S.W., K.M.M., T.T.P., and I.J.F. analyzed data; and L.R.M., I.F.G., S.-H.Y., M.S.W., T.T.P., and I.J.F. wrote the paper.

The authors declare no conflict of interest.

This article is a PNAS Direct Submission.

Freely available online through the PNAS open access option.

¹L.R.M. and I.F.G. contributed equally to this work.

²To whom correspondence may be addressed. Email: tpaull@utexas.edu or ifinkelstein@cm.utexas.edu.

This article contains supporting information online at www.pnas.org/lookup/suppl/doi:10.1073/pnas.1516674113/-DCSupplemental.

functional relationship between SOSS1 and RPA during hExo1 resection remains unresolved.

Here, we use high-throughput single-molecule DNA curtains and quantitative cell biology to reveal the interplay between human and yeast Exo1 and SSBs during DNA resection. We show that both human and yeast Exo1s are processive nucleases, but are rapidly stripped from DNA by RPA. RPA inhibition is dependent on its multiple DNA binding domains. Remarkably, SOSS1 and other SSBs with fewer than three DNA binding domains support long-range resection by hExo1. In human cells, depletion of RPA increases the rate of hExo1 recruitment to laser-induced DNA damage but reduces the extent of resection. In the presence of RPA, both human and yeast Exo1 can resect DNA using a distributive, multiple-turnover mechanism, potentially reconciling prior conflicting *in vitro* observations. Together, our work reveals the mechanistic basis for how RPA and SOSS1 differentially modulate hExo1 activity and highlights an additional, unexpected role for these SSBs in DNA resection. We anticipate that these findings will shed light on how Exo1 is regulated in multiple genome maintenance pathways.

Results

Visualizing Exo1-Catalyzed DNA Resection. We used high-throughput single-molecule DNA curtains to observe individual hExo1 enzymes (Fig. 1*A*). To measure DNA resection, we assembled arrays of DNA molecules (48.5 kb, derived from λ -phage) on the surface of a microfluidic flowcell. The flowcell was coated with a surface-

passivating fluid lipid bilayer, and the DNA substrate was affixed to the bilayer via a biotin-streptavidin linkage. Nanofabricated chrome barriers were used to organize thousands of DNA molecules for high-throughput data collection and analysis (28–30). As hExo1 has been reported to preferentially load on 3'-ssDNA ends (18, 31–33), we prepared a λ -phage DNA that contained a 72-nt 3'-polyT overhang. The surface-immobilized DNA was extended for fluorescent imaging via the application of mild buffer flow from a computer-controlled syringe pump (28). When tagged at the C terminus, hExo1 retains full biochemical activity *in vitro* and is active *in vivo*. Therefore, we purified the enzyme with a C-terminal biotinylation sequence from cells overexpressing biotin ligase (15, 34–36). Nearly 100% of the hExo1 molecules were biotinylated (as measured by streptavidin band-shift; Fig. S1). For fluorescent imaging, biotinylated hExo1 was conjugated to a large excess of streptavidin-labeled quantum dots (QDs), ensuring fewer than one enzyme per QD (37). Streptavidin conjugation did not impair hExo1 activity in either gel-based or single-molecule resection assays (Fig. S1).

Fluorescently labeled hExo1 was injected into the flowcell and visualized using total internal reflection fluorescence microscopy (TIRFM). We optimized protein injection conditions to load one or fewer fluorescent enzymes per DNA molecule (Fig. 1*B*; 4 nM hExo1 in imaging buffer consisting of 40 mM Tris-HCl, pH 8, 60 mM NaCl, 1 mM MgCl₂, 2 mM DTT, and 0.2 mg/mL bovine serum albumin (BSA)). Nearly all hExo1 molecules were bound to DNA, as turning off buffer flow led to the coordinated retraction

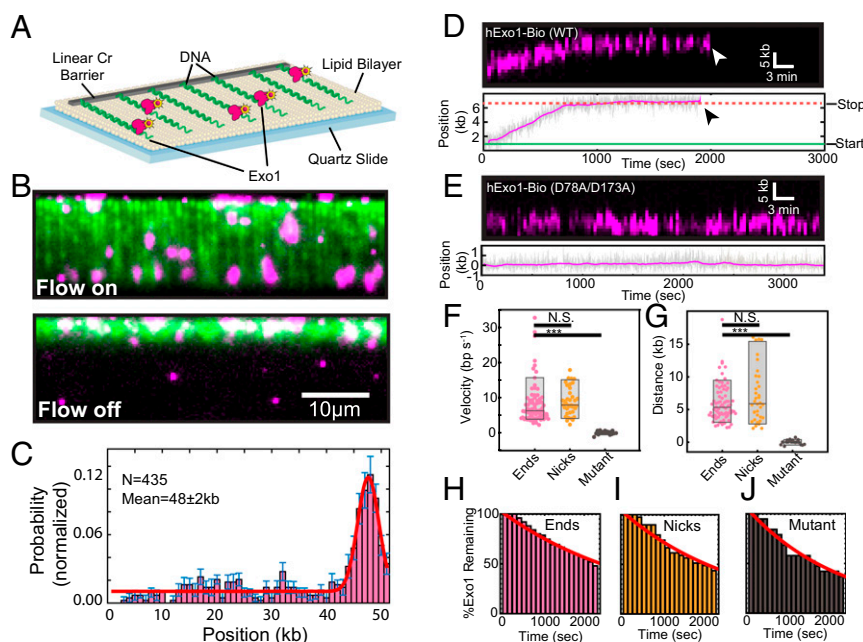


Fig. 1. hExo1 is a processive DNA nuclease. (A) Schematic of the DNA curtains assay with hExo1. The flowcell surface is passivated with a lipid bilayer. DNA is affixed to the lipid bilayer, organized at nano-fabricated barriers, and extended to ~85% of its B-form contour length. (B) Example of a DNA curtain (green) with fluorescent hExo1 molecules (magenta) in the presence (Upper) and absence (Lower) of buffer flow. Nearly all hExo1 molecules retracted with the DNA when buffer flow is turned off (Lower). (C) A histogram of the positions of individual hExo1 molecules bound to DNA ($n = 435$ molecules). The red line is a single-Gaussian fit to the data (the mean of the fit is 48 ± 2 kb), and the error bars indicate the SD obtained via bootstrap analysis (73). hExo1 preferentially binds the free 3'-ssDNA end but can also engage internal DNA sites. (D) Kymograph (Upper) and the corresponding particle-tracking trace (Lower) of a single hExo1 resecting from a DNA end (arrowhead indicates dissociation). (E) Kymograph (Upper) and corresponding trace (Lower) of nuclease-dead hExo1 (D78A/D173A). (F) Box plots of velocities of WT hExo1 from ends (magenta, mean velocity = 8.4 ± 5.9 bp/s, $n = 75$) and nicks (orange, mean velocity = 9.0 ± 3.9 bp/s, $n = 38$), as well as for the nuclease-dead mutant (black, mean velocity = 0.1 ± 0.5 bp/s, $n = 19$). (G) hExo1 is a processive nuclease from both ends (magenta, mean processivity = 6.0 ± 2.9 kb, $n = 75$) and nicks (orange, processivity = 7.2 ± 4.2 kb, $n = 36$). The nuclease-dead mutant does not move (black, processivity = 0.01 ± 0.3 kb, $n = 19$). The velocities and processivities from nicks and ends are statistically indistinguishable ($P = 0.57$ for velocities, $P = 0.09$ for processivities) but are different from the nuclease-dead mutant (black, $***P = 2.1 \times 10^{-8}$ for velocity, $***P = 2.7 \times 10^{-14}$ for processivity). Box plots indicate the median, 10th, and 90th percentiles of the distribution. (H–J) hExo1 lifetimes at ends ($n = 75$), nicks ($n = 39$), and with nuclease-dead hExo1 ($n = 19$). The red line is a single exponential fit to the data. As ~50% of the molecules still remained on the DNA after our 40-min observation window, we report the lower estimate of the hExo1 half-lives ($>1,800$ s for hExo1 and $>1,400$ s for nuclease-dead hExo1).

of both the DNA and associated hExo1 molecules to the diffusion barrier (Fig. 1*B*, Lower). To prevent the accumulation of additional nicks via DNA photodamage, we omitted intercalating DNA dyes in subsequent experiments. Next, we assayed hExo1-DNA binding specificity in the absence of nuclease activity (MgCl₂ was replaced with 2 mM EDTA; Fig. S2). Fifty-six percent of all hExo1 molecules ($n = 244/435$) localized to the vicinity of the 3'-ssDNA ends (Fig. 1*C*); the remaining nucleases were distributed at internal binding sites, consistent with hExo1's role in binding DNA nicks during MMR and NER (7, 38). These data indicate that individual hExo1 molecules preferentially bind 3'-ssDNA overhangs but can also bind rare DNA nicks (we estimate approximately three to five per DNA molecule) that occur as a result of handling the 48-kb-long λ -DNA substrates.

hExo1 Is a Processive Nuclease That Interconverts Between Two States During Resection. To track the position of individual resecting hExo1 molecules with subpixel accuracy, we fit the time-dependent fluorescent signals to a 2D Gaussian function (39). The resulting time-dependent trajectories were used to analyze movement by individual nucleases (Fig. 1*D*, Lower). Up to 70% of the molecules moved on DNA, whereas the remaining 30% of the molecules were stationary during the 2,400-s observation time. We also observed that moving hExo1 molecules could interconvert between two distinct modes: a paused state and a translocating state that was characterized by directional and processive movement along the DNA (Fig. 1*D*). As expected, nuclease-dead Exo1(D78A/D173A) bound at the 3'-ssDNA ends but did not move on DNA (mean velocity = 0.1 ± 0.5 bp/s; processivity = 0.01 ± 0.3 kb, $n = 19$; Fig. 1*E*) (32). We also did not observe any resection when EDTA was substituted for divalent metal ions (Fig. S2). We considered a translocating molecule to be paused if it moved less than our ~ 300 -bp resolution for at least 100 s. Seventy-one percent ($n = 53/75$) of DNA end-bound hExo1 molecules transitioned at least once between a translocating and a paused state; the remaining 29% ($n = 22/75$) of these molecules resected DNA without pausing. Of the molecules that paused at least once, 45% ($n = 24/53$) initially bound the DNA in a paused state before switching to processive movement (mean pause duration = 750 ± 380 s, $n = 24$). The majority of molecules that paused at least once (91%, $n = 48/53$) stopped before dissociating from DNA and did not restart DNA resection (mean pause duration = $1,070 \pm 770$ s, $n = 48$). We also observed two-state trajectories with a fluorescent anti-biotin antibody bound to hExo1-bio and with hExo1-Flag labeled with a single QD-conjugated anti-Flag antibody, indicating that both the paused and resecting states were not dependent on the nature of the fluorophore (Fig. S1*D* and Fig. S3). Stationary hExo1 may stem from protein inactivation during overexpression and purification or may be an intrinsic property of the enzyme. In support of the second model, a recent X-ray crystallographic study of hExo1 suggested that the largely unstructured C terminus, which is present in our full-length protein, harbors an auto-inhibitory domain (32). This domain interacts with hMSH2 and hMLH1 (40, 41) and is critical for hMutS α stimulation of hExo1 nuclease activity (5, 32, 42).

We next analyzed the time-dependent hExo1 trajectories to measure the velocity, processivity, and DNA-binding lifetime of each resecting enzyme. DNA end-bound hExo1 moved 6.0 ± 2.9 kb (range indicates SD, $n = 75$), with a mean velocity of 8.4 ± 5.9 bp/s (range indicates SD, $n = 75$) from DNA ends. From nicks, hExo1 moved 7.2 ± 4.2 kb ($n = 38$) with a mean velocity of 9.0 ± 3.9 bp/s ($n = 36$; Fig. 1*F* and *G*). As expected, the mean velocity and processivity were statistically indistinguishable with a different fluorescent label on hExo1 and at a higher ionic strength (Figs. S3 and S4). hExo1 velocity and processivity were statistically similar from both DNA ends and nicks ($P = 0.57$ for velocities, $P = 0.09$ for processivities) but very distinct from the nuclease-dead hExo1

($P = 2.1 \times 10^{-8}$ for velocities, $P = 2.7 \times 10^{-14}$ for processivities; Fig. 1*F* and *G*). Inverting the tethered and free DNA ends also yielded statistically similar velocity, processivity, and pause state distributions (Fig. S5), indicating that hExo1 resection is independent of the underlying DNA sequence. Furthermore, hExo1 associated tightly with the DNA (Fig. 1*H–J*). The dissociation half-life was similar for both end- and nick-bound hExo1 (half-life $>1,800$ s, $n = 75$ and 39 for ends and nicks, respectively) as well as with the nuclease-dead mutant (half-life $>1,400$ s, $n = 19$). We conclude that hExo1 is a processive nuclease that associates tightly with both nicks and free DNA ends.

RPA Inhibits hExo1 by Stripping the Nuclease from DNA. RPA rapidly associates with ssDNA and can modulate the activity of enzymes that participate in DNA resection (14, 43). To determine how human RPA (hRPA) affects hExo1, we first loaded hExo1 on DNA and then injected imaging buffer containing a low concentration (1 nM) of GFP-tagged hRPA (44). hRPA-GFP rapidly displaced hExo1 from the DNA as it loaded onto the newly generated ssDNA (Fig. 2*A*). There was no discernible difference in hExo1 displacement by hRPA-GFP compared with WT hRPA (Fig. S6). Injection of WT hRPA—but not storage buffer—also led to rapid hExo1 dissociation from the DNA (Fig. 2*C*; half-life = 18 ± 1 s, $n = 90$; error bars report 95% CI). Both stationary and moving hExo1s, as well as nuclease-dead hExo1(D78A/D173A) (Fig. S6*B*), were rapidly displaced by hRPA. Importantly, hRPA also inhibited resection by unlabeled hExo1, indicating that this inhibition was not due to the hExo1 labeling strategy (Fig. S7). RPA occludes ~ 30 nt when it engages ssDNA (14, 45). Therefore, the 78-nt ssDNA overhangs used in this study can bind, at most, two or three hRPA complexes. Our data indicates that this is sufficient to strip hExo1 from DNA.

Next, we investigated whether the RPA inhibition was species specific. We purified WT yeast RPA (yRPA) and determined its effect on hExo1. On injecting 1 nM yRPA into the flowcell, hExo1 was rapidly removed from the DNA (half-life = 40 ± 1 s, $n = 210$; Fig. S6*D*). Although both human and yeast RPA can displace hExo1, hRPA can do so twice as rapidly as the yeast protein (Table S1). Both RPA complexes have subnanomolar affinity for ssDNA, suggesting that hRPA may displace hExo1 by direct competition for the ssDNA and also via species-specific interactions (46, 47). These results are surprising, as a physical interaction between the human or yeast RPA and Exo1 has not been reported (15, 21). Nonetheless, the proximity of the two complexes on the same DNA strand can be sufficient to enhance weak but species-specific interactions. Here, we conclude that hRPA rapidly displaces hExo1 and that three or fewer hRPA complexes are sufficient to remove both stationary and resecting hExo1 from DNA.

SOSS1 Supports Processive Resection by hExo1. SOSS1 is required for extensive DSB resection in cells (24, 25) and strongly stimulates hExo1 loading onto free DNA ends (21). However, the mechanism by which SOSS1 regulates hExo1 resection remains unexplored. To determine how SOSS1 modulates hExo1, we purified a GST-tagged SOSS1 complex and fluorescently labeled it with an Alexa488-conjugated anti-GST antibody (21). Fluorescent SOSS1 was then injected into flowcells containing resecting hExo1 molecules. Alexa488-SOSS1 colocalized with hExo1 at both nicks and ends but surprisingly did not displace the nuclease from DNA (Fig. 2*B*). We next assayed hExo1 activity when 1 nM SOSS1 (without the fluorescent label) was introduced into the flowcell. In contrast to hRPA, SOSS1 supported long-range resection. hExo1 stayed on the DNA for tens of minutes (Fig. 2*D*; half-life $>2,000$ s, $n = 52$), and the dwell time, velocities, and processivities were statistically indistinguishable from those of hExo1 in the absence of any SSBs (Fig. 2*E*, $P = 0.16$ for velocities and $P = 0.14$ for processivities). In the presence of SOSS1, 92% ($n = 48/52$) of

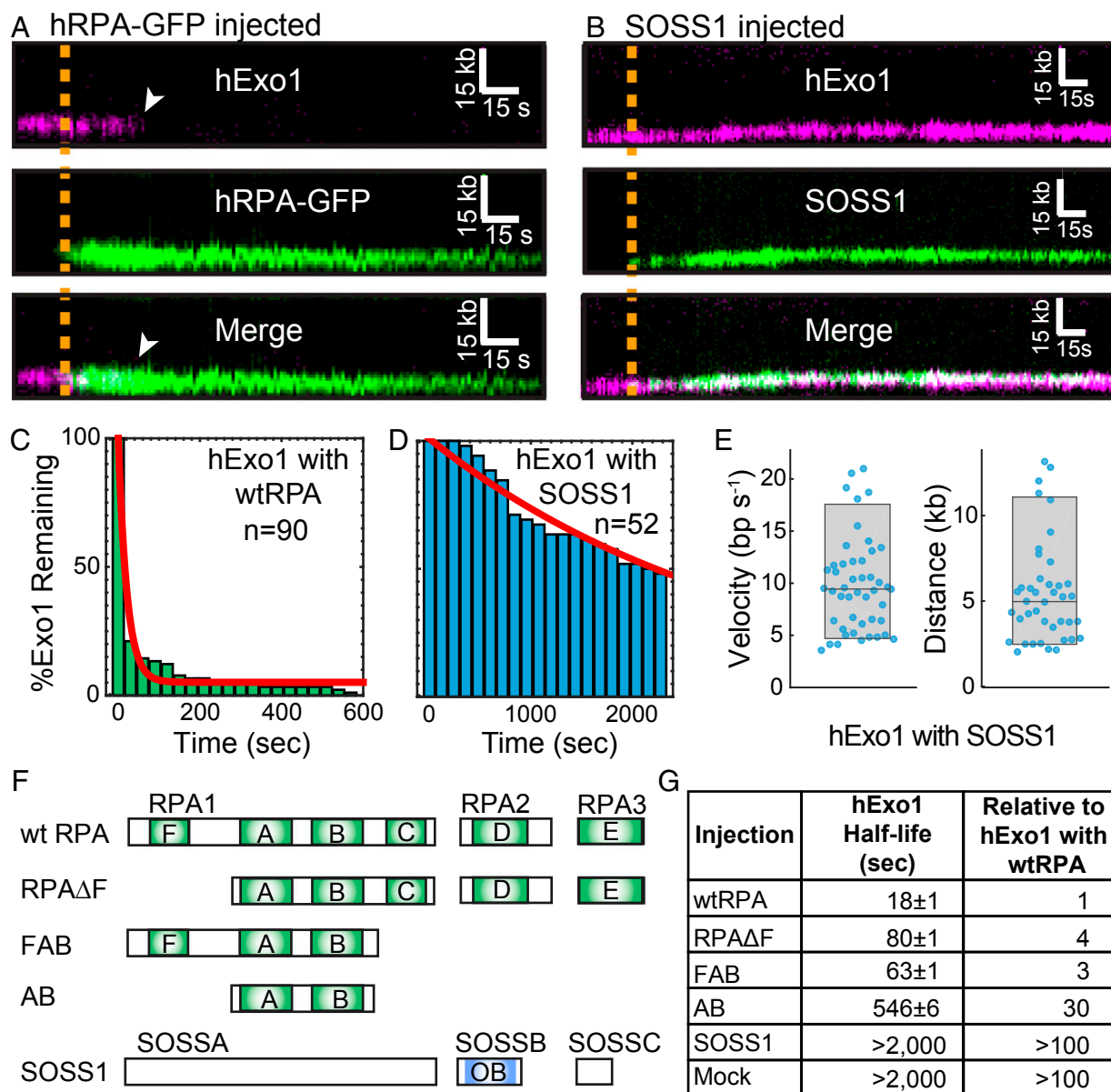


Fig. 2. RPA, but not SOSS1, rapidly dissociates hExo1 from DNA. (A) Kymograph of hExo1 displacement (magenta, *Top*) by hRPA-GFP (green, *Middle*). (*Bottom*) Merged images. The orange line indicates when hRPA-GFP enters the flowcell, and white arrowheads indicate hExo1 dissociation. (B) Kymograph of hExo1 (magenta, *Top*) with injection of fluorescent SOSS1 (green, *Middle*). (*Bottom*) Merged images, and the orange line indicates when SOSS1 entered the flowcell. (C) Lifetime of DNA end-bound hExo1 in the presence of 1 nM RPA (half-life = 18 ± 1 s, $n = 90$) and (D) 1 nM SOSS1 (half-life $>2,000$ s, $n = 52$). Red lines, single exponential fits to the data. (E) Distribution of hExo1 velocities (*Left*; 9.8 ± 4.5 bp/s, $n = 47$) and processivities (*Right*; 5.5 ± 3.0 kb, $n = 41$) with 1 nM SOSS1 in the imaging buffer. Box plots indicate the median, 10th, and 90th percentiles of the distributions. (F) Diagram of hRPA, SOSS1, and various truncations used in this study. DNA binding domains are shown in light green (hRPA) or blue (SOSS1). (G) Half-lives of hExo1 in the presence of several hRPA truncations, SOSS1, or a mock injection containing RPA storage buffer. Right column indicates the half-lives normalized to those of hExo1 with hRPA.

hExo1 trajectories transitioned at least once between a paused and a resecting state, mirroring our earlier observations with hExo1 in the absence of any SSBs. The remaining 8% of these molecules ($n = 4/52$) resected DNA without pausing. Of the molecules that paused at least once, 73% ($n = 35/48$) paused before resecting and 63% ($n = 30/48$) paused after DNA resection. We conclude that SOSS1 binds newly resected DNA without altering hExo1 velocity or processivity.

hExo1 Is Inhibited by Multivalent SSBs. We next sought to determine the mechanism by which RPA—but not SOSS1—displaces hExo1. RPA is composed of three polypeptides (RPA1, RPA2, and RPA3) that encode six nonequivalent DNA-binding domains

(DBDs A–F; Fig. 2*F*, *Upper*) (14, 47). Biochemical and cell biology studies with truncated proteins have established that DBD-A and DBD-B have the strongest ssDNA-binding affinities and are essential for proper RPA function in DNA replication and repair (16, 47, 48). RPA1 also encodes an N-terminal DBD-F, which is connected to the DBD-A/B via a long polypeptide linker, harbors a weak DNA binding activity, and physically interacts with DNA replication and repair proteins (45, 49, 50). To determine the key RPA domains that are required for hExo1 displacement, we purified and assayed a series of truncated hRPA variants (Fig. 2*F*). A heterotrimeric hRPA complex lacking DBD-F (RPAΔF) was able to displace hExo1 but at a fourfold slower rate than WT RPA (half-life = 80 ± 1 s, $n = 66$; Fig. S6*D*). Next, we tested a series of

RPA1 truncations that contained the high-ssDNA affinity DBD-A/B. Surprisingly, the FAB-RPA1 truncation was still proficient for hExo1 removal (half-life = 63 ± 1 s, $n = 37$) and could do so more efficiently than RPA Δ F (Fig. 2G and Fig. S6D). The N terminus of RPA1 facilitates melting of ss/dsDNA junctions and is also a central hub for many RPA-interacting proteins (49). Our data indicate that this domain may also help to displace hExo1 by two nonexclusive mechanisms: (i) direct competition for the ssDNA and (ii) weak physical interactions with the nuclease. In contrast, the minimal DBD-A/B RPA1 truncation, which contains just the two highest affinity ssDNA-binding domains, was 30-fold slower than WT hRPA at removing hExo1 from DNA (Fig. 2G and Fig. S6D; half-life = 546 ± 6 s; $n = 28$). Interestingly, the SOSS1 complex contains only a single DNA binding domain, which may be why it fails to displace hExo1.

Our finding that truncated hRPA variants that retain three DBDs may rapidly displace hExo1 suggested that other SSBs with multiple DNA-binding domains could also remove hExo1 from DNA. To further test this observation, we measured the rate of hExo1 removal by the homotetrameric *E. coli* SSB and monomeric T4 phage gp32 (Fig. S8). Injecting 1 nM *E. coli* SSB, which harbors four identical DBDs, rapidly inhibited hExo1, with a similar half-life to RPA Δ F (half-life = 74 ± 1.3 s, $n = 31$; Fig. S8C and Table S1). In contrast, gp32 did not rapidly strip hExo1 from DNA (half-life = 790 ± 90 s; $n = 34$; Fig. S8D). Moreover, neither gp32 nor SOSS1 affected the hExo1 resection rate and processivity (Fig. S8E and Fig. 2E). These results clarify earlier studies showing that SSB, but not gp32, can substitute for hRPA in limiting hExo1 resection in a reconstituted human MMR system (5). Here, we show that SSB and RPA, but not gp32, can both efficiently turn over resecting hExo1. The similarities between the dwell times of hExo1 in the presence of RPA Δ F and *E. coli* SSB suggest that multivalent SSBs can efficiently displace hExo1 from DNA but that the N terminus of hRPA1 may harbor an additional hExo1-regulating domain.

hRPA Depletion Increases hExo1 Recruitment to DNA Damage but Decreases Resection in Human Cells. Our single-molecule observations demonstrated that RPA inhibits hExo1-dependent DNA resection. To extend these findings *in vivo*, we established two assays for monitoring hExo1 recruitment to DNA damage sites in human cells. First, we measured the dynamics of hExo1-GFP recruitment to laser-induced DNA damage in hRPA-depleted cells. RPA2 knockdown stimulated the rate of hExo1-GFP recruitment to laser-induced DNA damage in U2OS cells (Fig. 3A–C). This effect was not due to changes in cell cycle progression because RPA2 knockdown did not appreciably alter the proportion of cells in S-phase (Fig. 3D and Fig. S9A). In addition, hExo1-GFP colocalized with γ -H2AX foci at the site of the laser damage (Fig. S9B). Overall, these results indicate that RPA inhibits hExo1 accumulation at DNA damage sites.

Next, we established a ChIP assay to monitor hExo1 localization at ssDNA intermediates in human cells. We adapted a resection assay using U2OS cells engineered to express an estrogen receptor ER-AsiSI restriction enzyme fusion that can be trafficked into the nucleus on treatment with 4-hydroxytamoxifen (4-OHT) (51, 52). AsiSI induction generates up to 150 DSBs per cell (51). Resection efficiency can be measured by quantitative PCR (qPCR) using two primers located downstream of two different AsiSI recognition sites on chromosome I that are known to be cleaved with high efficiency (12). Here, we extended this assay by stably integrating V5-epitope tagged hExo1 into the AsiSI-inducible U2OS cells. hExo1 recruitment to a DSB was monitored by ChIP with anti-V5 antibodies followed by qPCR to quantify the amount of DNA associated with hExo1. We detected more hExo1 associated with DNA in hRPA-depleted cells at both DSB-proximal (80 bp away) and distal (800 bp away) sites (Fig. 3E). These results were also consistent across two different AsiSI-generated DSBs.

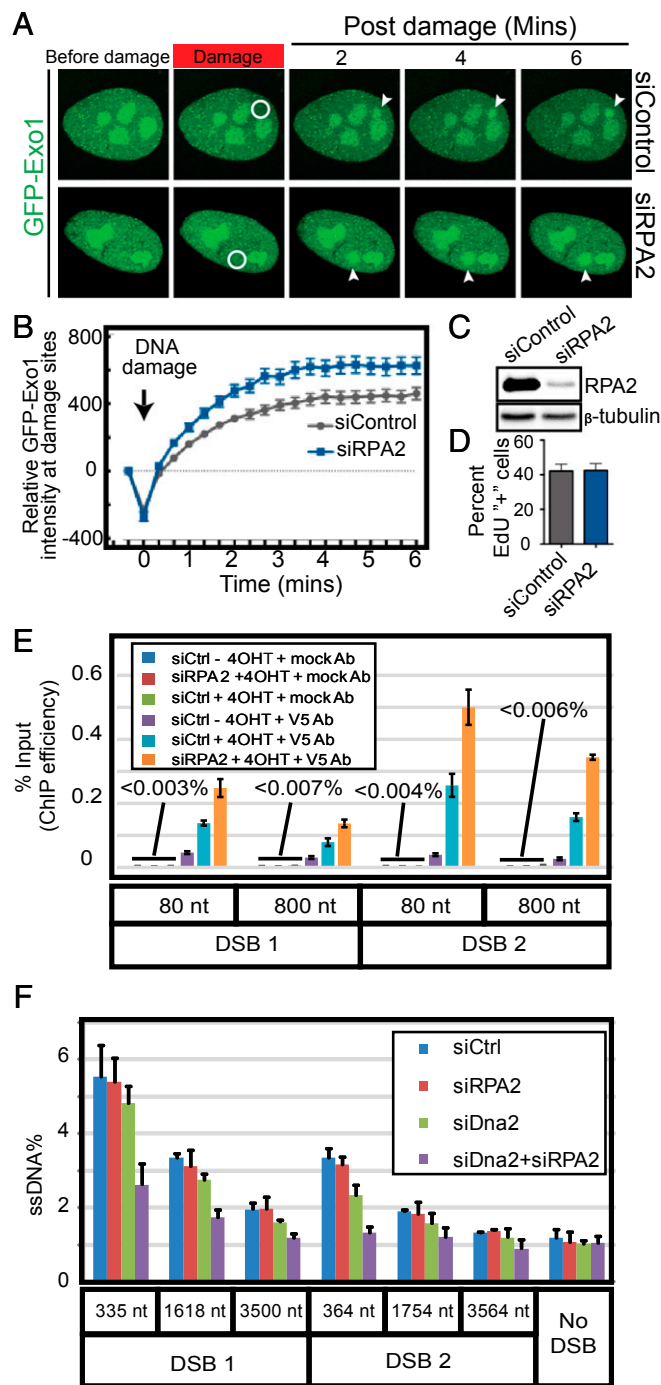


Fig. 3. hRPA depletion increases hExo1 localization to DNA break sites but decreases resection in human cells. (A) Representative images of laser-induced GFP-hExo1 foci in the presence of siControl or siRPA2. The white circle indicates site of laser damage. (B) Quantification of A with at least 20 cells per biological replicate. (C) Western blot showing levels of RPA2 after siRPA2 treatment. Loading control: β -tubulin. (D) Quantification of EdU⁺ cells (S phase) in the presence and absence of RPA2. (E) Quantification of hExo1 ChIP efficiency at DNA sites that are 80 or 800 nt downstream of two different AsiSI-induced breaks (DSB1 and DSB2). (F) qPCR-based resection assays were carried out with siControl-, siRPA2-, siDna2-, and siDna2+siRPA2-treated cells. All error bars indicate SEM from three biological replicates.

We conclude that depletion of hRPA leads to increased accumulation of hExo1 at DSBs, consistent with our laser irradiation experiments in cells and our *in vitro* single-molecule assays.

Next, we exploited the AsiSI-induced DSB assays to determine how hRPA coordinates DNA resection. ssDNA generation at specific sites near AsiSI-induced breaks was monitored by cleavage with restriction enzymes followed by qPCR with primers spanning those sites (53). Resection of DSB ends prevents restriction enzyme cleavage, allowing amplification of the DNA and quantification of the percentage of produced ssDNA. Using this assay, we have previously shown that hExo1 and SOSS1 both promote long-range resection of free DNA ends into ssDNA substrates (21). Here, we show that hRPA-depleted cells can still produce DNA resection intermediates up to ~ 3.5 kb away from the break site. Because hExo1 is the major nuclease in human DSB resection (11), hExo1 knockdown severely limits DNA resection intermediates (12). A second, partially redundant resection pathway requires DNA2 nuclease (19, 20, 22, 23). To specifically monitor hExo1-dependent resection, we first measured resection in DNA2-depleted cells. DNA2-depleted cells displayed only a minor DNA resection defect (11, 12). To define the role of hRPA on hExo1 resection, we next quantified DNA resection intermediates in cells that were depleted for both RPA2 and DNA2. Surprisingly, codepletion of RPA2 and DNA2 resulted in decreased ssDNA generation, suggesting additional roles for hRPA in regulating DNA resection (Fig. 3F) (15). Taken together, these results show that hRPA depletion enhances hExo1 recruitment to sites of DSBs in human cells, but long-range DSB processing is fine-tuned by additional components of the resection machinery.

yExo1 Is a Processive Nuclease. Early studies with purified human and yeast Exo1 reported that the enzymes act as distributive nucleases, whereas we observed processive resection with full-length hExo1 (Fig. 1) (6, 31, 54, 55). To determine whether the human and yeast enzymes are functionally similar, we also purified biotinylated yExo1 and observed its activity on DNA curtains at its optimal temperature (30 °C; Fig. 4A). As reported previously, yExo1 preferentially bound the free 3'-ssDNA ends (18). Similar to hExo1, we saw individual end-bound molecules transition between a paused and a translocating state (Fig. 4A). Seventy-eight percent of yExo1 molecules ($n = 45/58$) paused at least once, with the remaining 22% ($n = 13/58$) resecting without pausing. Forty-two percent of the molecules that paused ($n = 19/45$) showed pausing before translocation (mean pause time: 430 ± 170 s, $n = 19/45$). In addition, 93% of these molecules paused after translocation (mean pause time: $1,320 \pm 720$ s, $n = 42/45$). Unlike hExo1, however, only $\sim 12\%$ of total yExo1 molecules showed directional movement ($n = 58/490$); the remaining molecules were stationary on the DNA. Despite the large number of stationary nucleases, our single-molecule assay permits us to determine the velocity and processivity of moving yExo1 proteins. In the absence of SSBs, these molecules resected DNA with a similar velocity and processivity to hExo1 (mean velocity = 10.9 ± 5.4 bp/s, processivity = 5.6 ± 2.6 kb, $n = 57$; Fig. 4B and C). yExo1 remained on the DNA ends for $>1,800$ s (Fig. 4E; $n = 58$), as we had observed with hExo1. Consistent with the effect of hRPA on hExo1, injection of yRPA rapidly removed both stationary and resecting yExo1 from DNA ends (Fig. 4D and F; half-life = 52 ± 2 s, $n = 76$, $R^2 = 0.93$). We conclude that in these single-turnover assays, yExo1 is also a processive nuclease but is rapidly displaced from DNA by yRPA.

Exo1 Is a Distributive Nuclease in the Presence of RPA. Our previous data show that individual human and yeast Exo1 molecules are rapidly inhibited by RPA and that this inhibition is largely species independent. However, previous biochemical studies have reported that RPA can both stimulate and inhibit Exo1 (5, 18, 19, 21, 23, 31). To reconcile these results, we performed ensemble assays with varying concentrations of human or yeast Exo1 (Fig. 5A and B). Consistent with our single molecule data

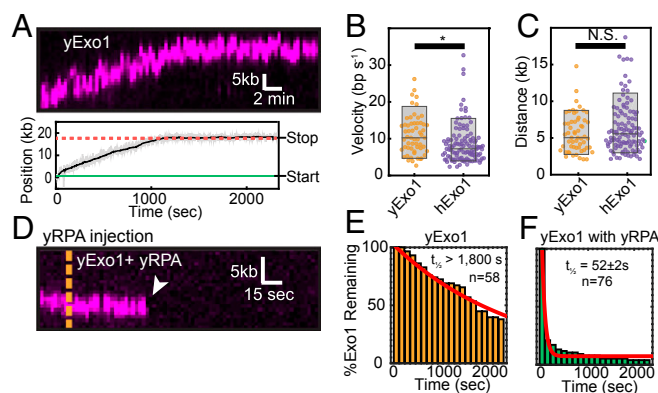


Fig. 4. yExo1 is a processive nuclease. (A) Kymograph (Upper) and resection track (Lower) showing yExo1 processing of a DNA end. (B) Comparison of yExo1 (orange) and hExo1 (purple) velocities ($n = 57$ for yExo1 and $n = 113$ for hExo1) and (C) processivities ($n = 57$ for yExo1 and $n = 111$ for hExo1). The P values were 0.004 and 0.15 for the velocities and processivities, respectively. For yExo1, the mean velocity was 10.9 ± 5.4 bp/s and the average processivity was 5.6 ± 2.6 kb ($n = 57$). (D) Kymograph of a yExo1 molecule in the presence of 1 nM yRPA. The orange line indicates when yRPA enters the flowcell. (E) yExo1 lifetimes in the absence of yRPA (orange, half-life $>1,800$ s; $n = 58$) and (F) with 1 nM yRPA injected into the flowcell (green, half-life = 52 ± 2 s, $n = 76$). The red lines are single exponential fits to the data.

(Fig. 2), hExo1 was strongly inhibited by hRPA at a range of concentrations and time points (Fig. 5A). Surprisingly, we found that yExo1 retained resection activity in the presence of yRPA and that this effect was dependent on the relative concentration of yExo1 and DNA substrate (Fig. 5B). We reasoned that resection could still occur in the presence of yRPA if yExo1 can reload at the same ss/dsDNA junction. Given that only $\sim 12\%$ of the DNA-bound yExo1 molecules were active in the single-molecule assay, yRPA may appear to stimulate resection in an ensemble gel assay by turning over both inactive and active enzymes (SI Discussion).

To test this model, we designed a single-molecule assay that mimics gel-based ensemble experiments and allows us to visualize multiple Exo1 rebinding events in the presence of RPA. For these experiments, 1 nM QD-labeled Exo1 was premixed with 1 nM RPA and injected for 10 min into a flowcell with preformed DNA curtains. The imaging buffer also contained 1 nM WT RPA. First, we quantified the amount of time that each Exo1 remained associated with the DNA (Fig. 5C and D). With both human and yeast Exo1, the distribution of dwell times was best described by two characteristic timescales that resulted in a sum of two exponential decays (as determined by an F -test; SI Experimental Procedures). The shorter timescale constituted 63% of the binding events for hExo1 (half-life = 0.9 ± 0.1 s, $n = 55$, $R^2 = 0.98$) and 73% of the events for yExo1 (half-life = 3.9 ± 0.2 s, $n = 62$, $R^2 = 0.99$). These short dwell times may correspond to Exo1 molecules that are evicted rapidly because RPA is already prebound on ssDNA when Exo1 encounters that DNA site. For both proteins, the longer timescale was similar to the dwell times that we observed when the corresponding RPA was injected in our single-turnover experiments (Fig. 2C for hExo1 and Fig. 4F for yExo1). Both binding modes were three times longer for yExo1 with yRPA than the corresponding human proteins. Loading events were also much more frequent, even at lower yExo1 concentrations. When we injected 0.2 nM yExo1, we saw ~ 0.5 yExo1 binding events per minute per DNA molecule ($n = 21$ DNA molecules). In contrast, we injected 2.5-fold more hExo1 (0.5 nM) but only saw ~ 0.2 hExo1 binding events per minute per DNA ($n = 37$ DNA molecules). Together with our single-turnover results (see previous section), these data suggest that yExo1

loads hExo1 on free DNA ends but does not otherwise stimulate processive nucleolytic resection.

RPA inhibits human and yeast Exo1, and possibly other nucleases and ssDNA-associated enzymes, by rapidly displacing them from DNA. We favor a mechanism where RPA can either diffuse for a short distance on ssDNA or bind directly behind Exo1 (Fig. 6) (57). Next, one of the low-affinity DBDs competes with Exo1 for the ssDNA directly downstream of the ss/dsDNA junction, causing disruption of Exo1–ssDNA interactions. An Exo1 hydrophobic wedge—found in all FEN1-family nucleases—makes critical contacts with at least three nucleotides of ssDNA (32, 58). We propose that one of the six RPA DBDs, likely DBD-F, interferes with Exo1–ssDNA contacts to displace Exo1 from DNA. Our results, in concert with other biochemical studies indicating that RPA also inhibits Fen1 at Okazaki fragment flaps and Pot1 at telomeric DNA (59–62), suggest a general mechanism where RPA physically strips other proteins from DNA. Indeed, we demonstrate that the tetrameric *E. coli* SSB can strip hExo1 from DNA (Fig. S8). Likewise, SSB limits the processivity of the AdnAB helicase nuclease, and archeal SSB limits the activity of XPF nuclease (63, 64). These observations are consistent with a general mechanism whereby multivalent SSBs can regulate the dissociation, and thus the processivity, of diverse families of nucleases.

Because RPA is ubiquitous in eukaryotic cells, how does Exo1 resect long tracts of DNA during HR and MMR? Several groups have reported a growing list of additional proteins that promote Exo1 activity. For example, hMutS α forms a sliding clamp and physically interacts with hExo1 to stimulate lesion-provoked excision during MMR (32, 65). The hMutS α –hExo1 complex may be more resistant to removal by hRPA (4, 32, 42). In addition, Bowen et al. reported that mismatch-provoked

resection by scExo1 was limited in the presence of scRPA, but was strongly stimulated by scMutS α (66). During HR, hExo1 is stimulated by the protein complex Mre11/Rad50/Nbs1 (Nibrin), (MRN), BLM, and proliferating cell nuclear antigen (PCNA)—all of which physically interact with hExo1 and may help to retain the nuclease on DNA (19, 21, 36). Furthermore, we have shown that in the presence of RPA, both human and yeast Exo1 can rebind the same DNA site multiple times, suggesting a distributive resection mechanism (Fig. 5). This mechanism could be beneficial to cells when Exo1 stalls or is blocked (e.g., at a nucleosome), which would require removal from DNA for reloading and repair to continue (67).

RPA depletion leads to an increased hExo1 localization at both laser-induced DNA damage and at restriction enzyme-generated DSBs in human cells (Fig. 3). Our results in human cells are broadly consistent with a recent study on the role of RPA during DSB resection in yeast (15). RPA depletion in both human and yeast cells inhibited the production of ssDNA tracts, suggesting additional roles for RPA in facilitating end resection. RPA recruits the kinase ATR to DSBs, which promotes resection via phosphorylation of histone H2AX, C-terminal binding protein interacting protein, (CtIP), and Rad17 (67–71). As hExo1 cannot resect past a nucleosome in vitro (66), RPA may also be required for recruiting chromatin remodelers to the DSB ahead of the resection machinery. Exo1 is also subject to a growing list of posttranslational modifications and is positively and negatively regulated by MRN, BLM, CtIP, and other components of the resection machinery (10, 21, 31, 35, 36). Our work provides a framework for future studies to determine how these interactions facilitate long-range DNA resection by Exo1 in the presence of RPA.

Experimental Procedures

All single-molecule measurements were conducted at 30 °C or 37 °C in imaging buffer containing 40 mM Tris-HCl (pH 8.0), 60 mM NaCl, 1 mM MgCl₂, 2 mM DTT, and 0.2 mg/mL BSA. For experiments at a higher ionic strength, the NaCl concentration was increased to 130 mM. Human or yeast Exo1-biotin was pre-labeled with streptavidin QDs (Qdot 705; Life Tech) before use, as previously described (72). To make the DNA curtain, λ -DNA was hybridized with a biotinylated oligonucleotide on one end and a 3' overhang-generating oligonucleotide on the other end (Table S2). hExo1-Flag was first injected into preassembled DNA curtains, excess protein was flushed out, and the remaining DNA-bound hExo1-Flag was labeled with 1 nM QD-conjugated anti-Flag M2 antibodies (Sigma) in situ. SOSS1 was pre-labeled with Alexa488-labeled antiGST antibodies (Cell Signaling #3368). In single-turnover experiments, human or yeast Exo1 was initially injected into the sample chambers and allowed to bind to the DNA. Unbound Exo1 proteins were then flushed away, and data collection was immediately initiated. All SSBs were injected at a concentration of 1 nM 1 min after hExo1 loading. For multiple-turnover experiments, 1 nM h/yExo1 and 1 nM h/yRPA with indicated fluorophores were injected continuously during data collection.

Two-color imaging was conducted using two electron-multiplying charge coupled device (EMCCD) cameras and a 638-nm dichroic beam splitter (Chroma). Position distribution measurements and particle tracking were conducted as previously described (29). Error bars on the binding distribution histogram represents the SDs of each bin in the histogram, as obtained through bootstrap analysis of the molecule binding data (29). For all processivities and velocities, we report the mean and SDs. The lifetimes of individual molecules were defined as the time hExo1 remained on the DNA after SSBs (or mock storage buffer) were injected into the flowcell. At least 30 nuclease molecules were analyzed for each condition, and the resulting survival histogram was fit with a single exponential decay to extract the half-life. The errors bars of the half-lives represent the 95% CI of the fit of the exponential time constant. Additional information is available online in *SI Experimental Procedures*.

ACKNOWLEDGMENTS. We thank Dr. Jennifer Surtees and members of the I.J.F., K.M.M., and T.T.P. laboratories for useful discussions and for critically reading the manuscript. We thank our colleagues Eric Greene (Columbia University, NY), Paul Modrich (Duke University, NC), R. Michael Liskay (Oregon Health & Science University, OR), Junjie Chen (MD Anderson Cancer Center, TX), and Mauro Modesti (Cancer Research Center of Marseille,

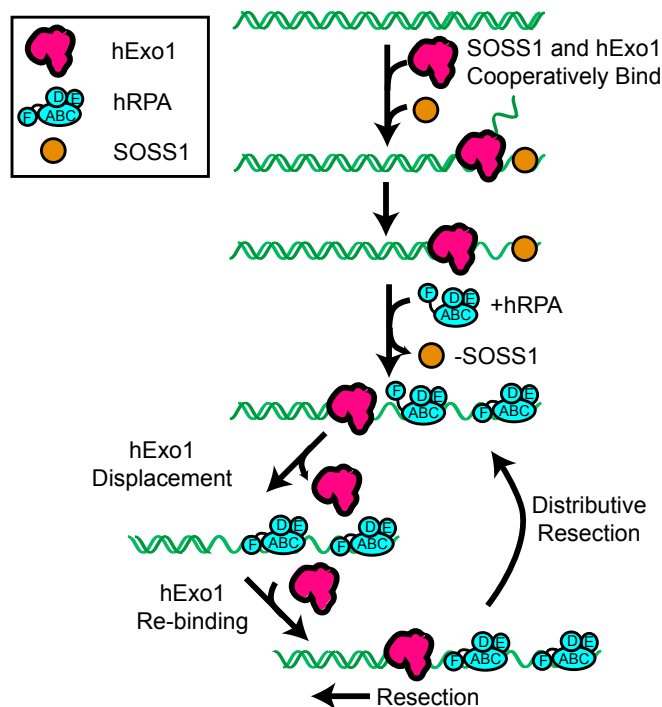


Fig. 6. A model for hExo1 regulation by human SSBs. SOSS1 cooperatively loads hExo1 on DNA ends. As hExo1 resects the DNA, SOSS1 is replaced by hRPA. hRPA displaces hExo1, but another hExo1 molecule can rebind at the site. This cycle of binding, displacement, and rebinding results in distributive resection. Additional factors (e.g., BLM, MRN, and PCNA; not included for clarity) may also promote resection in the presence of hRPA.

FR) for valuable reagents. This work was supported by National Institute of General Medical Sciences of the National Institutes of Health Grant GM097177 (to I.J.F.), the Cancer Prevention Research Institute of Texas

(CPRIT) Grants R1214 (to I.J.F.), R1116 (to K.M.M.), and RP110465 (to T.T.P.), and Welch Foundation Grant F-808 (to I.J.F.). I.J.F. and K.M.M. are CPRIT Scholars in Cancer Research.

- Mimitou EP, Symington LS (2011) DNA end resection—Unraveling the tail. *DNA Repair (Amst)* 10(3):344–348.
- Goellner EM, Putnam CD, Kolodner RD (2015) Exonuclease 1-dependent and independent mismatch repair. *DNA Repair (Amst)* 32:24–32.
- Tran PT, Erdeniz N, Symington LS, Liskay RM (2004) EXO1—A multi-tasking eukaryotic nuclease. *DNA Repair (Amst)* 3(12):1549–1559.
- Genschel J, Bazemore LR, Modrich P (2002) Human exonuclease I is required for 5' and 3' mismatch repair. *J Biol Chem* 277(15):13302–13311.
- Genschel J, Modrich P (2003) Mechanism of 5'-directed excision in human mismatch repair. *Mol Cell* 12(5):1077–1086.
- Szankasi P, Smith GR (1995) A role for exonuclease I from *S. pombe* in mutation avoidance and mismatch correction. *Science* 267(5201):1166–1169.
- Shao H, Baitinger C, Soderblom EJ, Burdett V, Modrich P (2014) Hydrolytic function of Exo1 in mammalian mismatch repair. *Nucleic Acids Res* 42(11):7104–7112.
- Liberti SE, Rasmussen LJ (2004) Is hEXO1 a cancer predisposing gene? *Mol Cancer Res* 2(8):427–432.
- Wei K, et al. (2003) Inactivation of Exonuclease 1 in mice results in DNA mismatch repair defects, increased cancer susceptibility, and male and female sterility. *Genes Dev* 17(5):603–614.
- Eid W, et al. (2010) DNA end resection by CtIP and exonuclease 1 prevents genomic instability. *EMBO Rep* 11(12):962–968.
- Tomimatsu N, et al. (2012) Exo1 plays a major role in DNA end resection in humans and influences double-strand break repair and damage signaling decisions. *DNA Repair (Amst)* 11(4):441–448.
- Zhou Y, Caron P, Legube G, Paull TT (2014) Quantitation of DNA double-strand break resection intermediates in human cells. *Nucleic Acids Res* 42(3):e19–e19.
- Tong AHY, et al. (2004) Global mapping of the yeast genetic interaction network. *Science* 303(5659):808–813.
- Wold MS (1997) Replication protein A: A heterotrimeric, single-stranded DNA-binding protein required for eukaryotic DNA metabolism. *Annu Rev Biochem* 66(1):61–92.
- Chen H, Lisby M, Symington LS (2013) RPA coordinates DNA end resection and prevents formation of DNA hairpins. *Mol Cell* 50(4):589–600.
- Hass CS, Lam K, Wold MS (2012) Repair-specific functions of replication protein A. *J Biol Chem* 287(6):3908–3918.
- Lisby M, Barlow JH, Burgess RC, Rothstein R (2004) Choreography of the DNA damage response: Spatiotemporal relationships among checkpoint and repair proteins. *Cell* 118(6):699–713.
- Cannavo E, Cejka P, Kowalczykowski SC (2013) Relationship of DNA degradation by *Saccharomyces cerevisiae* exonuclease 1 and its stimulation by RPA and Mre11-Rad50-Xrs2 to DNA end resection. *Proc Natl Acad Sci USA* 110(18):E1661–E1668.
- Nimonkar AV, et al. (2011) BLM-DNA2-RPA-MRN and EXO1-BLM-RPA-MRN constitute two DNA end resection machineries for human DNA break repair. *Genes Dev* 25(4):350–362.
- Niu H, et al. (2010) Mechanism of the ATP-dependent DNA end-resection machinery from *Saccharomyces cerevisiae*. *Nature* 467(7311):108–111.
- Yang S-H, et al. (2013) The SOSS1 single-stranded DNA binding complex promotes DNA end resection in concert with Exo1. *EMBO J* 32(1):126–139.
- Cejka P, et al. (2010) DNA end resection by Dna2-Sgs1-RPA and its stimulation by Top3-Rmi1 and Mre11-Rad50-Xrs2. *Nature* 467(7311):112–116.
- Nicolette ML, et al. (2010) Mre11-Rad50-Xrs2 and Sae2 promote 5' strand resection of DNA double-strand breaks. *Nat Struct Mol Biol* 17(12):1478–1485.
- Richard DJ, et al. (2008) Single-stranded DNA-binding protein hSSB1 is critical for genomic stability. *Nature* 453(7195):677–681.
- Huang J, Gong Z, Ghosal G, Chen J (2009) SOSS complexes participate in the maintenance of genomic stability. *Mol Cell* 35(3):384–393.
- Ren W, et al. (2014) Structural basis of SOSS1 complex assembly and recognition of ssDNA. *Cell Reports* 6(6):982–991.
- Richard DJ, et al. (2011) hSSB1 rapidly binds at the sites of DNA double-strand breaks and is required for the efficient recruitment of the MRN complex. *Nucleic Acids Res* 39(5):1692–1702.
- Finkelstein IJ, Greene EC (2011) Supported lipid bilayers and DNA curtains for high-throughput single-molecule studies. *Methods Mol Biol* 745:447–461.
- Finkelstein IJ, Visnapuu M-L, Greene EC (2010) Single-molecule imaging reveals mechanisms of protein disruption by a DNA translocase. *Nature* 468(7326):983–987.
- Robison AD, Finkelstein IJ (2014) High-throughput single-molecule studies of protein-DNA interactions. *FEBS Lett* 588(19):3539–3546.
- Nimonkar AV, Oszoy AZ, Genschel J, Modrich P, Kowalczykowski SC (2008) Human exonuclease 1 and BLM helicase interact to resect DNA and initiate DNA repair. *Proc Natl Acad Sci USA* 105(44):16906–16911.
- Orans J, et al. (2011) Structures of human exonuclease 1 DNA complexes suggest a unified mechanism for nuclease family. *Cell* 145(2):212–223.
- Liao S, Guay C, Toczylowski T, Yan H (2012) Analysis of MRE11's function in the 5'→3' processing of DNA double-strand breaks. *Nucleic Acids Res* 40(10):4496–4506.
- Tran PT, Erdeniz N, Dudley S, Liskay RM (2002) Characterization of nuclease-dependent functions of Exo1p in *Saccharomyces cerevisiae*. *DNA Repair (Amst)* 1(11):895–912.
- Tomimatsu N, et al. (2014) Phosphorylation of EXO1 by CDKs 1 and 2 regulates DNA end resection and repair pathway choice. *Nat Commun* 5:3561.
- Chen X, Paudyal SC, Chin RI, You Z (2013) PCNA promotes processive DNA end resection by Exo1. *Nucleic Acids Res* 41(20):9325–9338.
- Pathak S, Davidson MC, Silva GA (2007) Characterization of the functional binding properties of antibody conjugated quantum dots. *Nano Lett* 7(7):1839–1845.
- Sertic S, et al. (2011) Human exonuclease 1 connects nucleotide excision repair (NER) processing with checkpoint activation in response to UV irradiation. *Proc Natl Acad Sci USA* 108(33):13647–13652.
- Thompson RE, Larson DR, Webb WW (2002) Precise nanometer localization analysis for individual fluorescent probes. *Biophys J* 82(5):2775–2783.
- Schmutte C, et al. (1998) Human exonuclease I interacts with the mismatch repair protein hMSH2. *Cancer Res* 58(20):4537–4542.
- Schmutte C, Sadoff MM, Shim K-S, Acharya S, Fishel R (2001) The interaction of DNA mismatch repair proteins with human exonuclease I. *J Biol Chem* 276(35):33011–33018.
- Genschel J, Modrich P (2009) Functions of MutLalpha, replication protein A (RPA), and HMG1 in 5'-directed mismatch repair. *J Biol Chem* 284(32):21536–21544.
- Chen R, Wold MS (2014) Replication protein A: Single-stranded DNA's first responder: Dynamic DNA-interactions allow replication protein A to direct single-strand DNA intermediates into different pathways for synthesis or repair. *BioEssays* 36(12):1156–1161.
- Modesti M (2011) Fluorescent labeling of proteins. *Methods Mol Biol* 783:101–120.
- Brosey CA, et al. (2013) A new structural framework for integrating replication protein A into DNA processing machinery. *Nucleic Acids Res* 41(4):2313–2327.
- Kim C, Snyder RO, Wold MS (1992) Binding properties of replication protein A from human and yeast cells. *Mol Cell Biol* 12(7):3050–3059.
- Wyka IM, Dhar K, Binz SK, Wold MS (2003) Replication protein A interactions with DNA: Differential binding of the core domains and analysis of the DNA interaction surface. *Biochemistry* 42(44):12909–12918.
- Haring SJ, Mason AC, Binz SK, Wold MS (2008) Cellular functions of human RPA1. Multiple roles of domains in replication, repair, and checkpoints. *J Biol Chem* 283(27):19095–19111.
- Binz SK, Wold MS (2008) Regulatory functions of the N-terminal domain of the 70-kDa subunit of replication protein A (RPA). *J Biol Chem* 283(31):21559–21570.
- Glanzer JG, et al. (2013) A small molecule directly inhibits the p53 transactivation domain from binding to replication protein A. *Nucleic Acids Res* 41(3):2047–2059.
- Iacovoni JS, et al. (2010) High-resolution profiling of gammaH2AX around DNA double strand breaks in the mammalian genome. *EMBO J* 29(8):1446–1457.
- Miller KM, et al. (2010) Human HDAC1 and HDAC2 function in the DNA-damage response to promote DNA nonhomologous end-joining. *Nat Struct Mol Biol* 17(9):1144–1151.
- Zhou Y, Paull TT (2015) Direct measurement of single-stranded DNA intermediates in mammalian cells by quantitative polymerase chain reaction. *Anal Biochem* 479:48–50.
- Fiorentini P, Huang KN, Tishkoff DX, Kolodner RD, Symington LS (1997) Exonuclease I of *Saccharomyces cerevisiae* functions in mitotic recombination in vivo and in vitro. *Mol Cell Biol* 17(5):2764–2773.
- Wilson DM, 3rd, et al. (1998) Hex1: A new human Rad2 nuclease family member with homology to yeast exonuclease 1. *Nucleic Acids Res* 26(16):3762–3768.
- Gibb B, et al. (2014) Concentration-dependent exchange of replication protein A on single-stranded DNA revealed by single-molecule imaging. *PLoS One* 9(2):e87922.
- Nguyen B, et al. (2014) Diffusion of human replication protein A along single-stranded DNA. *J Mol Biol* 426(19):3246–3261.
- Tsutakawa SE, et al. (2011) Human flap endonuclease structures, DNA double-base flipping, and a unified understanding of the FEN1 superfamily. *Cell* 145(2):198–211.
- Liu Y, Kao H-I, Bambara RA (2004) Flap endonuclease 1: A central component of DNA metabolism. *Annu Rev Biochem* 73(1):589–615.
- Ray S, Bandaria JN, Qureshi MH, Yildiz A, Balci H (2014) G-quadruplex formation in telomeres enhances POT1/TPP1 protection against RPA binding. *Proc Natl Acad Sci USA* 111(8):2990–2995.
- Rossi ML, et al. (2008) Pif1 helicase directs eukaryotic Okazaki fragments toward the two-nuclease cleavage pathway for primer removal. *J Biol Chem* 283(41):27483–27493.
- Bae S-H, Bae K-H, Kim J-A, Seo Y-S (2001) RPA governs endonuclease switching during processing of Okazaki fragments in eukaryotes. *Nature* 412(6845):456–461.
- Unciuleac MC, Shuman S (2010) Double strand break unwinding and resection by the mycobacterial helicase-nuclease AdnAB in the presence of single strand DNA-binding protein (SSB). *J Biol Chem* 285(45):34319–34329.
- Roberts JA, White MF (2005) DNA end-directed and processive nuclease activities of the archaeal XPF enzyme. *Nucleic Acids Res* 33(20):6662–6670.
- Gradia S, et al. (1999) hMSH2-hMSH6 forms a hydrolysis-independent sliding clamp on mismatched DNA. *Mol Cell* 3(2):255–261.
- Bowen N, et al. (2013) Reconstitution of long and short patch mismatch repair reactions using *Saccharomyces cerevisiae* proteins. *Proc Natl Acad Sci USA* 110(46):18472–18477.
- Adkins NL, Niu H, Sung P, Peterson CL (2013) Nucleosome dynamics regulates DNA processing. *Nat Struct Mol Biol* 20(7):836–842.
- Couch FB, et al. (2013) ATR phosphorylates SMARCAL1 to prevent replication fork collapse. *Genes Dev* 27(14):1610–1623.
- Driscoll R, Cimprich KA (2009) HARPing on about the DNA damage response during replication. *Genes Dev* 23(20):2359–2365.
- Peterson SE, et al. (2013) Activation of DSB processing requires phosphorylation of CtIP by ATR. *Mol Cell* 49(4):657–667.

71. Shiotani B, et al. (2013) Two distinct modes of ATR activation orchestrated by Rad17 and Nbs1. *Cell Reports* 3(5):1651–1662.
72. Lee JY, Finkelstein IJ, Crozat E, Sherratt DJ, Greene EC (2012) Single-molecule imaging of DNA curtains reveals mechanisms of KOPS sequence targeting by the DNA translocase FtsK. *Proc Natl Acad Sci USA* 109(17):6531–6536.
73. Efron B, Tibshirani RJ (1993) *An Introduction to the Bootstrap* (Chapman and Hall/CRC, New York).
74. Beckett D, Kovaleva E, Schatz PJ (1999) A minimal peptide substrate in biotin holoenzyme synthetase-catalyzed biotinylation. *Protein Sci* 8(4):921–929.
75. Horn R (1987) Statistical methods for model discrimination. Applications to gating kinetics and permeation of the acetylcholine receptor channel. *Biophys J* 51(2):255–263.
76. Shee C, et al. (2013) Engineered proteins detect spontaneous DNA breakage in human and bacterial cells. *eLife* 2:e01222.
77. Gong F, et al. (2015) Screen identifies bromodomain protein ZMYND8 in chromatin recognition of transcription-associated DNA damage that promotes homologous recombination. *Genes Dev* 29(2):197–211.
78. Leung JW, et al. (2014) Nucleosome acidic patch promotes RNF168- and RING1B/BMI1-dependent H2AX and H2A ubiquitination and DNA damage signaling. *PLoS Genet* 10(3):e1004178.
79. Aymard F, et al. (2014) Transcriptionally active chromatin recruits homologous recombination at DNA double-strand breaks. *Nat Struct Mol Biol* 21(4):366–374.